Kinetics and Catalysis, Vol. 42, No. 5, 2001, pp. 679–685. Translated from Kinetika i Kataliz, Vol. 42, No. 5, 2001, pp. 747–753.
Original Russian Text Copyright © 2001 by Zakharchenko.

Catalytic Properties of the Fe_2O_3–MnO System for Ammonia Oxidation

N. I. Zakharchenko

Zhukovskii State Aerospace University, Kharkov, Ukraine

Received May 5, 2000

Abstract—The effect of the chemical and phase composition of the Fe_2O_3–MnO catalytic system for ammonia oxidation on its activity and selectivity to NO at 873–1273 K is demonstrated. The optimal parameters of the process over manganese ferrite, the most active and highly selective component of the system, are determined. The combination of the factors of chemical and phase transformations of the catalyst results in the formation of an inactive component (Fe_3O_4) and in the structural changes (recrystallization and cationic redistribution of spinel) and is the reason for the deactivation of manganese ferrite at 1273 K.

INTRODUCTION

The catalytic oxidation of ammonia to NO is the basis for the industrial process for the production of nitric acid [1]. High cost, deficiency, and irreparable loss in the technological process of commercial catalyst (platinum, rhodium, and palladium alloys) production raise the topical problem of searching for efficient nonplatinum catalysts. Iron(III) oxide is one of the promising sources of nonplatinum catalysts and is used as a component of a combined system at the second stage of ammonia oxidation [1, 2]. Different modifiers, in particular, metal oxides are used to retain the high activity and selectivity of Fe_2O_3 to NO and to enhance its thermal and chemical stability [1–6]. Information about the catalysts for ammonia oxidation is empirical, because the current theory of catalysis fails to unambiguously predict the properties of catalysts depending on their composition, methods of preparation, and genesis. The accumulation of knowledge on the catalytic properties of systems for ammonia oxidation is of practical and theoretical interest for developing scientific methods for the preparation of catalysts with certain characteristics. Mn(II) oxide is used as a modifier for iron oxide-containing catalysts. However, the Fe_2O_3–MnO system has not been studied in a wide range of component compositions [1, 3, 4]. This paper is devoted to the study of catalytic properties of the Fe_2O_3–MnO system in ammonia oxidation.

EXPERIMENTAL

The catalyst was prepared by the thermal decomposition of hydrated iron ($Fe(NO_3)_3 \cdot 9H_2O$) and manganese ($Mn(NO_3)_2 \cdot 6H_2O$) nitrates (analytical grade) in the inert medium of N_2. The components were taken in a ratio calculated by the procedure [5, 7] that involved an additional thermal treatment of a catalyst at 1173 K for 6 h. The X-ray diffraction analysis was carried out with an URS-50I diffractometer using FeK_α radiation. The phase composition of the catalytic system under examination is presented in Table 1.

The specific surface areas of catalysts measured from the nitrogen low-temperature adsorption or calculated by the BET equation are summarized in Table 2.

The selectivities of catalysts to NO were determined in a flow-type setup (Fig. 1) with a quartz reactor 20 mm in diameter following the procedure reported in [8]. Once ammonia-air mixture was cleaned of impurities, it entered the reactor with a 40-mm fixed bed of catalyst granules 2×3 mm in size. The ammonia con-

Table 1. Phase composition of the Fe_2O_3–MnO system

MnO concentration, wt %	Phase composition	Properties of the system components	
		crystalline structure	lattice spacing *a*, nm
0	α-Fe_2O_3	trigonal, α-Al_2O_3-type	0.5430
0–30.7	α-Fe_2O_3 + $MnFe_2O_4$	–	–
30.8	$MnFe_2O_4$	cubic, $MgAl_2O_4$-type	0.8515
30.9–99.9	$MnFe_2O_4$+ MnO	–	–
100.0	MnO	cubic, NaCl-type	0.4435

0023-1584/01/4205-0679$25.00 © 2001 MAIK “Nauka / Interperiodica”

centration in the ammonia–air mixture was ~10 vol %, a contact time of 7.6×10^{-2} s was optimal according to data obtained earlier in [5], and the pressure of the mixture was 0.101 MPa. After passing through a cooler, an oxidizing agent, and a condenser, nitrous gases were absorbed by an alkaline solution. The required temperature was maintained in the reactor with a tubular electric furnace. The temperature of the tests (1053 K) corresponded to that at which the selectivity of a single-component iron oxide catalyst exhibited the highest selectivity [7]. The composition of ammonia oxidation and NO decomposition products over catalysts was determined by chromatography using the known procedure [9]. The concentrations of NH_3, O_2, N_2, NO, and N_2O in the gas mixture were found before and after its contact with catalysts. The detection limits of this analytical method for NH_3, NO, and for each of O_2, N_2, and N_2O were 3.0×10^{-3}, 3.5×10^{-3}, and 5.0×10^{-3} vol %, respectively.

The catalyst capacity limit toward ammonia conversion in an ammonia–air mixture was determined by procedure proposed by Temkin [3], which consisted in an increase in the catalyst capacity to the critical state of catalyst "quenching," that is, in the disturbance of the catalyst thermal balance after the transition of the reaction from diffusion-controlled to kinetic regime.

Kinetic characteristics of the reaction were determined using the temperatures of ferrite catalyst "ignition" and "quenching," that is, temperatures in critical points. To calculate the reaction rate, we used the procedure for the determination of the temperature range of external diffusion using the effect of catalyst quenching by decreasing the temperature of the ammonia–air mixture [10]. The temperature of the catalyst surface was measured from the bottom of the ammonia–air mixture flow with a chromel–alumel thermocouple pressed in the catalyst pellet (Fig. 2). The catalyst pellet was a cylinder 6 mm in diameter and 5 mm in height. The thermocouple was pressed into the pellet 0.3 mm from its top end. A layer of manganese ferrite granules 2–3 mm in size was placed between the pellet and reactor walls to compensate for the loss of heat by the catalyst to the surrounding medium by means of thermal radiation. The temperature of the ammonia–air mixture

Table 2. Properties of the Fe_2O_3–MnO catalytic system

MnO concentration, wt %	Specific surface area, m^2/g	Catalyst selectivity to NO, % ($\tau = 7.6 \times 10^{-2}$ s)	Catalyst capacity limit toward ammonia conversion $NH_3(\times 10^{-3})$, $m^3\ NH_3\ h^{-1}\ m^{-2}$	Ammonia breakthrough under critical conditions of catalyst quenching, rel %
0	5.9	94.7	6.50	0.30
2.0	6.0	94.8	6.54	0.29
5.0	6.1	94.8	6.60	0.29
10.0	6.2	94.9	6.70	0.28
15.0	6.3	95.0	6.78	0.28
20.0	6.4	95.1	6.90	0.27
25.0	6.6	95.1	7.04	0.26
28.0	6.7	95.2	7.12	0.25
30.0	6.7	95.2	7.22	0.25
30.8	6.8	95.2	7.25	0.25
32.0	6.7	93.9	7.10	0.27
35.0	6.5	89.8	6.88	0.31
37.0	6.4	86.5	6.76	0.33
40.0	6.1	83.7	6.50	0.38
45.0	5.7	78.8	6.10	0.45
50.0	5.3	73.8	5.74	0.53
60.0	4.7	65.0	5.10	0.68
70.0	4.0	56.9	4.42	0.82
80.0	3.4	50.0	3.74	0.95
85.0	3.1	46.6	3.48	1.02
90.0	2.8	43.1	3.14	1.08
95.0	2.6	40.2	2.88	1.13
98.0	2.5	38.8	2.72	1.17
100.0	2.4	38.2	2.62	1.20

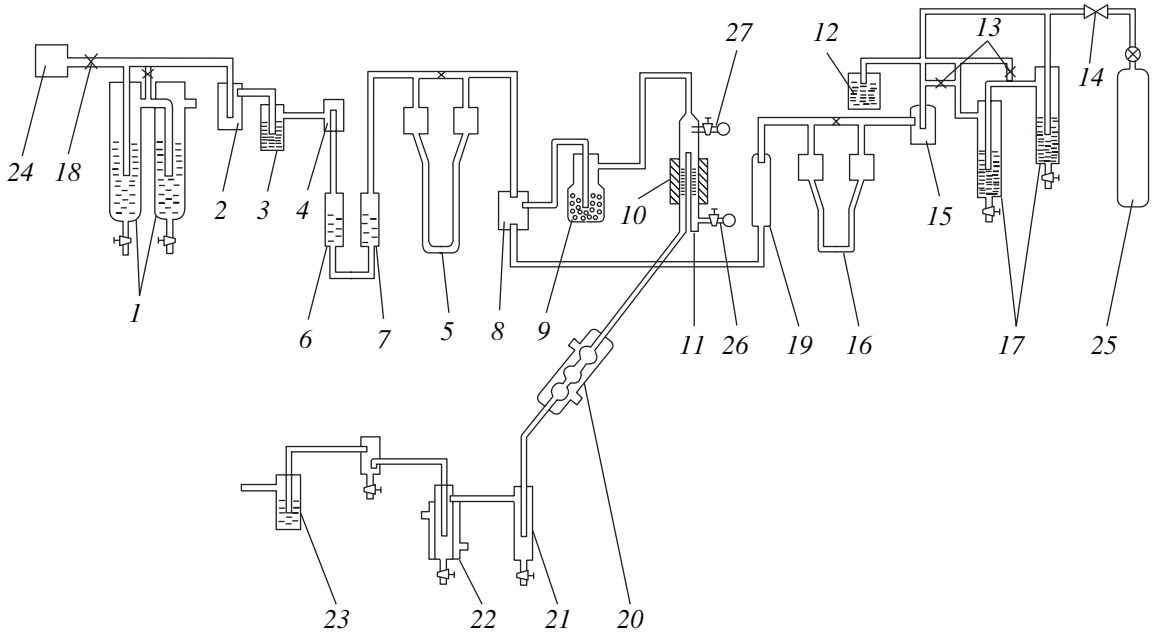

Fig. 1. Schematic of the setup for ammonia catalytic oxidation: (*1*, *17*) monostats; (*2*, *4*, *15*) traps; (*3*) Drechsel bottle with concentrated H_2SO_4; (*5*, *16*) rheometers; (*6*) filter with silica gel; (*7*) activated carbon; (*8*, *9*) mixers; (*10*) electric furnace; (*11*) reactor; (*12*) Drechsel bottle with an absorber (H_2O); (*13*, *14*, *18*) valves; (*19*) fiber-glass filter; (*20*) cooler; (*21*) oxidant; (*22*) condenser; (*23*) bottle with an absorber of nitrous gases (alkaline); (*24*) compressor; (*25*) cylinder with ammonia; (*26*, *27*) sampling valves.

that arrived at the pellet was measured with a chromel–alumel thermocouple surrounded with a layer of quartz granules [10] which are necessary to decrease the effect of the heat radiation from the pellet surface to the thermocouple.

RESULTS AND DISCUSSION

The catalytic properties of the Fe_2O_3–MnO system are presented in Fig. 3 and Table 2.

Only two nitrogen-containing compounds (N_2 and NO) were detected in the products of ammonia oxidation. No ammonia breakthrough was detected at the reactor output when the conditions were far from critical. Thus, the conversion of the initial substance was 100%. In the course of the reaction, only the concentration ratio between NO and molecular nitrogen changed, that is, the selectivity of catalysts to NO (or nitrogen) changed. The thermal dissociation of NO may result in a decrease in the selectivity to NO:

$$2NO = N_2 + O_2. \quad \text{(I)}$$

Experimental data on the extent of the thermal dissociation of NO over the catalysts of the system under study are presented in Table 3.

At a given temperature of experiments and during the optimal contact time ($\tau = 7.6 \times 10^{-2}$ s), from 0.4 to 1.0% NO dissociated. Thus, the thermal dissociation of NO reduced the selectivity of Fe_2O_3, MnO, and manganese ferrite catalysts to NO by 0.9, 0.1, and 1.1%, respectively. With an increase in the linear flow rate of reactants, that is, with a decrease in the contact time to 1.2×10^{-3} s (critical conditions of catalyst quenching), the thermal dissociation of NO was not detected. This pattern agrees with data obtained for other nonplatinum catalysts for ammonia oxidation [1, 11].

The addition of manganese oxide to hematite Fe(III) oxide (α-Fe_2O_3) led to the formation of manganese ferrite ($MnFe_2O_4$) with the structure of partially inverted spinel $Mn^{2+}_{0.9}Fe^{3+}_{0.1}[Mn^{3+}_{0.1}Fe^{2+}_{0.1}Fe^{3+}_{1.8}]O_4$ (the main lines of X-ray patterns corresponded to the following interplanar distances: 0.301; 0.257; 0.213; 0.1739; 0.1640; 0.1507; 0.1297; 0.1228; 0.1137; 0.1109; and 0.1065 nm) [12]. Data of chemical analysis and IR spectroscopic data (the main absorption bands were observed at 395 and 553 cm^{-1}) confirmed the composition of manganese ferrite.

At concentrations of manganese oxide higher than 30.8 wt %, the ferrite phase coexisted with the phase of manganese oxide as a mixture of two compounds. MnO showed the much lower selectivity (38.2%) and the specific surface area (2.4 m^2/g) than manganese ferrite. For example, an increase in the manganese oxide concentration in the $MnFe_2O_4$–MnO system resulted in a monotonic decrease in the selectivity of catalysts to NO. Thus, the selectivity of the system depended on its composition, in particular, on the quantitative ratio between the ferrite phase and one of the oxide phases of a binary catalyst.

The values of catalyst capacity limits based on ammonia are summarized in Table 2. It is seen that

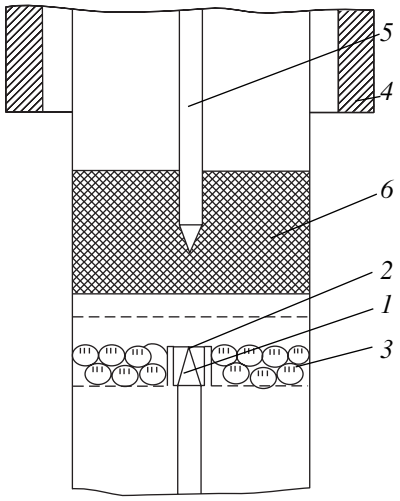

Fig. 2. Unit of the catalytic reactor for measuring kinetic characteristics of manganese ferrite: (*1*) catalyst pellet; (*2*) thermocouple for measuring the temperature of the catalyst surface; (*3*) bed of catalyst granules; (*4*) tube electric furnace; (*5*) thermocouple for measuring the temperature of ammonia–air mixture; (*6*) layer of quartz granules.

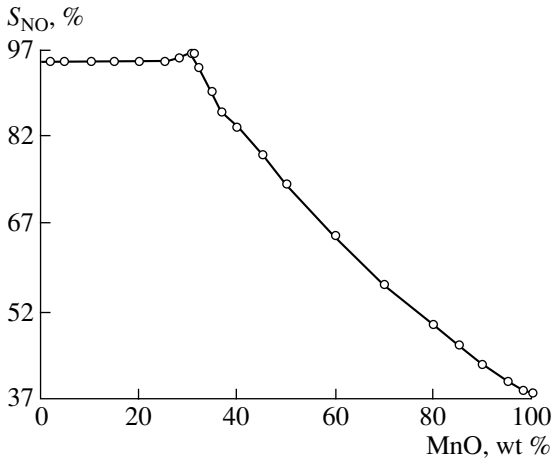

Fig. 3. Selectivity of catalysts to NO (S_{NO}, %) as a function of the composition of the Fe_2O_3–MnO system.

this parameter increased with an increase in their specific surface areas: manganese ferrite exhibited the highest capacity toward ammonia conversion (7.25×10^3 m^3 NH_3 h^{-1} m^{-2}) and Mn(II) oxide showed the lowest one (2.62×10^3 m^3 NH_3 h^{-1} m^{-2}). Iron(III) oxide showed a somewhat lower capacity limit than the manganese ferrite (6.50×10^3 m^3 NH_3 h^{-1} m^{-2}). The value of the capacity limit depends on the rate of a chemical reaction at the catalyst surface, which, in turn, is governed by the chemical composition of catalyst. The value of capacity limit characterizes the activity of catalysts and their maximal productivity [1, 13]. Thus, the activity of the Fe_2O_3–MnO system increased with an increase in its specific surface area. Under critical conditions of the process, all active sites of the catalyst are used, and their number increased with an increase in the specific surface area of the system. We state that both the specific surface area of catalyst and its chemical nature are responsible for the high catalytic activity of the Fe_2O_3–MnO system. Under critical conditions of the process ($\tau = 1.2 \times 10^{-3}$ s), the consecutive decomposition of NO by reaction (I) was not observed (Table 3), but part of unreacted ammonia was detected at the reactor output, that is, ammonia breakthrough took place (Table 2). With an increase in the specific surface area of catalysts, the ammonia breakthrough decreased. This fact is in agreement with a higher activity of such catalysts.

Manganese ferrite is the most selective and active component in the Fe_2O_3–MnO catalytic system for ammonia oxidation. The catalytic properties of manganese ferrite have not been studied previously.

Figure 4 demonstrates the effect of the reaction temperature on the selectivity of manganese ferrite to NO (henceforth, selectivity).

Manganese ferrite exhibited a higher selectivity than Fe(III) oxide at 873–1273 K; that is, it is an efficient catalyst for ammonia oxidation at moderate and high temperatures [1, 3, 4]. The temperature–selectivity curves for manganese ferrite and Fe(III) oxide were similar and characterized by a single maximum (Fig. 4). The selectivity maximum of manganese ferrite (95.4%) was shifted to higher temperatures compared to hematite (1103 and 1053, respectively). In addition, the temperature range (983–1193 K) of high selectivity (~94.0%) was wider for manganese ferrite than for Fe(III) oxide for which it was only 50–60 K.

The relation between the selectivity and the contact time (Fig. 5) pointed to the complex mechanism of ammonia oxidation [1, 5] over manganese ferrite.

At a time of contact (τ) shorter than 8×10^{-3} s, a drastic decrease in the catalyst selectivity was due to the side reaction [1, 15]

$$4NH_3 + 6NO = 5N_2 + 6H_2O. \quad \text{(II)}$$

At a time of contact longer than $\tau > 3.8 \times 10^{-2}$ s, a slow decrease in selectivity was mainly caused by the dissociation of NO by reaction (I) [1].

The linear flow rate of reactants (ammonia–air mixture) had a considerable effect on the catalyst selectivity (Fig. 6). According to [1, 3–5], this was typical of the external diffusion-controlled mechanism of the process, when the reaction rate was limited by ammonia diffusion from the flow to the manganese ferrite surface.

For manganese ferrite, the optimal linear flow rate of the ammonia–air mixture at $\tau = 3.6 \times 10^{-2}$ s was 0.80 m/s. An increase in the linear flow rate of reactants was accompanied by a shift of the hot zone to the end of the catalyst bed, that is, in a decrease in the temperature of its front layer. Thus, at $w = 1.8$ m/s, the temper-

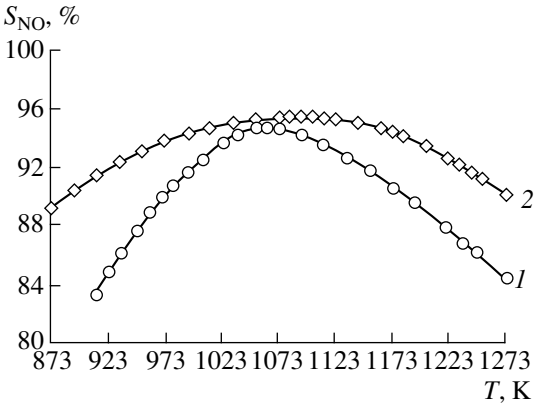

Fig. 4. Selectivity of catalysts to NO (S_{NO}, %) as a function of the process temperature: (*1*) α-Fe_2O_3 [14]; (*2*) $MnFe_2O_4$; the linear flow rate of ammonia–air mixture was 0.8 m/s.

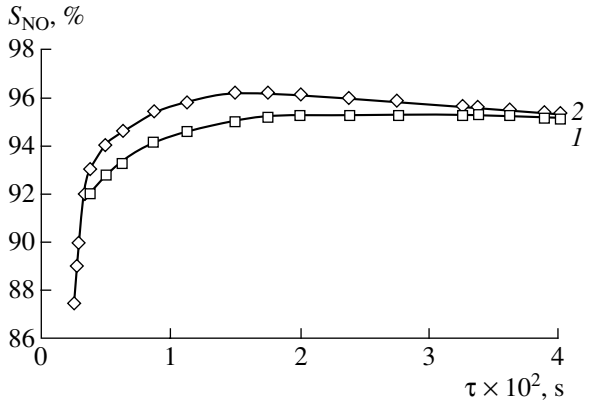

Fig. 5. Selectivity of manganese ferrite to NO (S_{NO}, %) as a function of the time of contact (τ) at 1103 K (the linear flow rate of ammonia–air mixture was (*1*) 0.8 and (*2*) 1.6 m/s).

ature of the catalyst front layer decreased to 873 K, which favored the occurrence of the parallel reaction

$$4NH_3 + 3O_2 = 2N_2 + 6H_2O. \qquad \text{(III)}$$

This reaction resulted in a decrease in the selectivity of manganese ferrite to NO (Fig. 4) and in the contribution of the consecutive process (II). Specifically, the rate of reaction (II) was maximal in the temperature range from 673 to 873 K [1, 15].

An increase in the linear flow rate of reactants to critical values resulted in the catalyst quenching, that is, in the disturbance of the heat balance of the process caused by a drastic increase in heat loss. The catalyst capacity limit toward ammonia conversion was 7.25×10^3 m^3 NH_3 h^{-1} m^{-2} and characterized the activity and productivity of manganese ferrite [1, 13]. When the process was performed under critical conditions, the consecutive decomposition of NO was poorly observed (Table 3), but part of unreacted ammonia broke through the catalyst layer at high linear flow rates of reactants (Table 2).

Kinetic data on the process were calculated by the equation proposed by Buben [16] and solved for two reaction rates at a constant concentration of oxygen. Buben's equation has the following form:

$$(1 + a)^2\left[1 + (m - 1)\frac{a}{b}\right] - \frac{a}{\varepsilon}\left(1 - \frac{a}{b}\right) = 0, \qquad (1)$$

where $a = \frac{T}{T_0} - 1$; $b = \frac{Q\beta C_0}{\alpha T_0}$; $\varepsilon = \frac{RT_0}{E}$; m is the reaction order with respect to ammonia; T is the temperature of the catalyst surface in a critical point, K; T_0 is the temperature of ammonia–air mixture; C_0 is the concentration of ammonia in the flow; α and β are the coefficients of mass and heat transfer, respectively; Q is the reaction heat; and E is the activation energy of the reaction.

Coefficients α and β were calculated from the known equations [17].

The kinetic parameters of ammonia oxidation over manganese ferrite are given below.

The temperature of catalyst ignition	530 K
The ammonia concentration in the ammonia–air mixture	10.0 vol %
The activation energy of reaction (E)	9.61 kJ/mol
The reaction order with respect to ammonia	0.20
The catalyst selectivity to NO (1053 K)	95.2%

The study of the catalyst selectivity changes with time (Fig. 7) pointed to the high stability of manganese ferrite at 1073–1173 K.

For 160 h, the selectivity of manganese ferrite at 1073 and 1173 K decreased by 0.2 and 0.4%, respectively. The selectivity of Fe_2O_3 at 1073 K decreased by 3.5% for the same period of time [7]. An increase in temperature to 1273 K resulted in the deactivation of manganese ferrite in the presence of reaction mixture;

Table 3. Degree of NO decomposition over catalysts at 1053 K (the gas mixture contained (vol %) 9.5 NO, 71.3 N_2, 4.6 O_2, and 14.6 H_2O (vapor)

MnO concentration, wt %	Degree of NO decomposition at a contact time of 7.6×10^{-2} s, %*
0 (α-Fe_2O_3)	1.0
15.0 (α-Fe_2O_3 + $MnFe_2O_4$)	1.1
30.8 ($MnFe_2O_4$)	1.2
60.0 ($MnFe_2O_4$ + MnO)	0.6
100.0 (MnO)	0.4

* The thermal dissociation of NO at a contact time of 1.2×10^{-3} s was not detected.

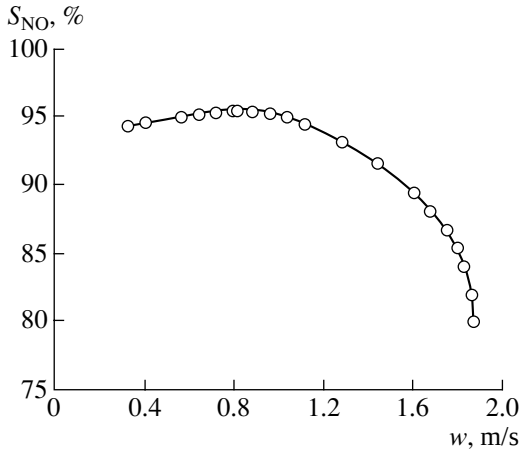

Fig. 6. Selectivity of manganese ferrite to NO (S_{NO}, %) as a function of the linear flow rate of ammonia–air mixture (w) at $\tau = 3.6 \times 10^{-2}$ s and $T = 1103$ K.

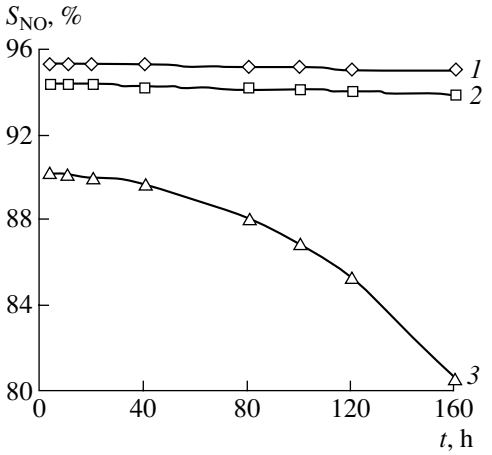

Fig. 7. Selectivity of manganese ferrite to NO (S_{NO}, %) as a function of the time of catalyst operation (t) at (*1*) 1073, (*2*) 1173, and (*3*) 1273 K (the linear flow rate of ammonia–air mixture (w) was 0.8 m/s).

a 9.5% decrease in the catalyst selectivity was observed after 160 h. X-ray patterns of the catalyst after 160 h at 1273 K contained the lines of manganese ferrite and the lines corresponding to interplanar distances typical of magnetite (Fe_3O_4) [12]: 0.485, 0.297, 0.253, 0.242, 0.2101, 0.1712, 0.1614, and 0.1485 nm. This conclusion was supported by IR spectroscopic data. IR spectra of the surface layer of the catalyst taken after its use exhibited the absorption bands of magnetite [18] (407, 427, 480, 557, 673, and 980 cm^{-1}). According to [7], magnetite decreased the selectivity of the catalyst and was an inactive phase (the selectivity of magnetite at 1073 K was 7.0%). In addition, the catalyst underwent essential structural changes. A decrease in the parameter of a crystal lattice (α) from 0.8515 to 0.8501 nm observed after 60 h at 1273 K was typical of the redistribution of cations in the spinel structure of manganese ferrite [19–21]. At 1273 K, the intense migration of Mn^{2+} ions from tetrahedral to octahedral sublattice was observed. This corresponded to a higher degree of the spinel inversion that occurred by the following equation [19, 20] (according to the data of XRD analysis and magnetic moments of the catalyst, it grew from 10 to 20%):

$$Mn^{2+}_{0.9}Fe^{3+}_{0.1}[Mn^{3+}_{0.1}Fe^{2+}_{0.1}Fe^{3+}_{1.8}]O_4 \longrightarrow Mn^{2+}_{0.8}Fe^{3+}_{0.2}[Mn^{3+}_{0.2}Fe^{2+}_{0.2}Fe^{3+}_{1.6}]O_4. \quad \text{(IV)}$$

In the tetrahedral sublattice, the high-temperature redox process [21, 22]

$$Mn^{2+} + Fe^{3+} \longrightarrow Mn^{3+} + Fe^{2+}, \quad \text{(V)}$$

whose equilibrium shifted to the right at 1273 K was according to the Jahn–Teller effect [19, 20, 22]. Such an electron exchange resulted in a decrease in the parameter of the spinel lattice [20, 21] in agreement with our observation.

Structural conversions of the spinel at 1273 K in the presence of the reaction mixture enhanced the probability of the chemical and phase transformations of manganese ferrite with the formation of an inactive magnetite phase [21, 22]. In addition, the catalyst was recrystallized at high temperatures and its specific surface area decreased (Table 4). Catalyst grains increased in size from 300 to 700 nm after its 160-h operation.

Because the reaction was limited by ammonia diffusion to the external surface of the catalyst, the value of specific surface area had no decisive effect on the manganese ferrite selectivity to NO [1, 3, 4]. This means that a decrease in the catalyst selectivity at 1273 K was mainly caused by phase and chemical transformations of the catalyst. Under critical conditions of the reaction (catalyst quenching), the processes of recrystallization and a decrease in the specific surface area resulted in a decrease in the capacity limit of manganese ferrite, that is, in a decrease in its activity (Table 4).

Table 4. Changes of some structural and catalytic characteristics of manganese ferrite during its operation at 1273 K

Time of operation, h	Specific surface area, m^2/g	Size of particles, nm	Catalyst capacity limit toward ammonia conversion NH_3 ($\times 10^{-3}$), $m^3\ NH_3\ h^{-1}\ m^{-2}$
10	5.6	300	6.00
40	4.0	380	4.25
60	2.3	520	2.44
100	0.9	680	0.97
160	0.8	700	0.86

The combination of chemical and phase transformations of the catalyst that resulted in the formation of a low-activity component and in the structural changes of the catalyst was the reason for the deactivation of manganese ferrite at 1273 K.

Data on the catalytic properties of the Fe_2O_3–MnO system can be used to develop efficient modified catalysts for ammonia oxidation.

REFERENCES

1. Karavaev, M.M., Zasorin, A.P., and Kleshchev, N.F., *Kataliticheskoe okislenie ammiaka* (Catalytic Oxidation of Ammonia), Moscow: Khimiya, 1983.
2. Epshtein, D.A., Tkachenko, I.M., Dobrovol'skaya, N.V., *et al.*, *Dokl. Akad. Nauk SSSR*, 1958, vol. 122, no. 5, p. 874.
3. Morozov, N.M., Luk'yanova, L.I., and Temkin, M.I., *Kinet. Katal.*, 1966, vol. 7, no. 1., p. 172.
4. Kurin, N.M. and Zakharov, M.S., *Kataliz v vysshei shkole* (Catalysis in Higher School), Balandin, A.A., Ed., Moscow: Mos. Gos. Univ., 1962, vol. 2, p. 234.
5. Zakharchenko, N.I. and Seredenko, V.V., *Zh. Prikl. Khim.*, 1999, vol. 72, no. 11, p. 1921.
6. USSR Inventor's Certificate no. 1182721, *Byull. Izobret.*, 1984, no. 14.
7. Zasorin, A.P., Zakharchenko, N.I., and Karavaev, M.M., *Izv. Vyssh. Uchebn. Zaved., Ser. Khim. Khim. Tekhnol.*, 1980, vol. 23, no. 10, p. 1274.
8. *Analiticheskii kontrol' proizvodstva v azotnoi promyshlennosti* (Analytical Control in Nitrogen Industry), Demin, L.A., Ed., Moscow: Goskhimizdat, 1958.
9. Alkhazov, T.G., Gasan-zade, G.Z., Osmanov, M.O., and Sultanov, M.Yu., *Kinet. Katal.*, 1975, vol. 16, no. 16, p. 1230.
10. Beskov, V.S., Karavaev, M.M., Garov, D.V., and Arutyunyan, V.A., *React. Kinet. Catal. Lett.*, 1976, vol. 4, no. 3, p. 351.
11. Zhidkov, B.A., Orlova, S.S., Bochenko, G.A., and Plygunov, A.S., *Khim. Tekhnol.*, 1979, no. 1, p. 5.
12. *Powder Diffraction Data, ASTM, Joint Committee in Powder Diffraction Standards*, Philadelphia, 1967.
13. Mukhlenov, I.P., Dobkina, E.I., Deryuzhkina, V.I., and Soroka, V.E., in *Tekhnologiya katalizatorov* (Catalyst Technology), Mukhlenov, I.P., Ed., Leningrad: Khimiya, 1989.
14. Zasorin, A.P. and Zakharchenko, N.I., Manuscript no 166—KhP D80 available from ONIITEKhIM, Cherkassy, 1980.
15. Ganz, S.N. and Vashkevich, A.M., *Zh. Prikl. Khim.*, 1970, vol. 43, no. 1, p. 13.
16. Buben, N.Ya., *Zh. Fiz. Khim.*, 1945, vol. 19, nos. 4–5, p. 250.
17. Kasatkin, A.G., *Osnovnye protsessy i apparaty khimicheskoi tekhnologii* (Basic Processes and Apparatus in Chemical Technology), Moscow: Khimiya, 1973.
18. Bogdanovich, N.P., Vorob'ev, Yu.P., Men', A.N., *et al.*, *Opt. Spektrosk.*, 1970, vol. 29, no. 6, p. 1151.
19. Talanov, V.M., *Energeticheskaya kristallokhimiya mnogopodreshetochnykh kristallov* (Energetic Crystallochemistry of Many-Sublattice Crystals), Rostov-on-Don: Rostov Univ., 1986.
20. Levin, B.E., Tret'yakov, Yu.D., and Letyuk, L.M., *Fiziko-khimicheskie osnovy polucheniya, svoistva i primeneniya ferritov* (Physicochemical Fundamentals of Ferrite Preparation, Their Properties, and Uses), Moscow: Metallurgiya, 1979.
21. Karpasyuk, V.K., Kiselev, V.M., Orlov, G.M., and Shchepetkin, A.A., *Elektromagnitnye svoistva i nestekhiometrichnost' ferritov s pryamougol'noi petlei gisterezisa* (Electromagnetic Properties of Nonstoichiometric Ferrites with Rectangular Hysteresis Loops), Moscow: Nauka, 1985.
22. Reznitskii, L.A., *Khimicheskaya svyaz' i prevrashcheniya oksidov* (Chemical Bonds and Oxide Transformations), Moscow: Moscow State University, 1991.